Journal of Marine Systems 239 (2023) 103858

Contents lists available at ScienceDirect

Journal of Marine Systems

journal homepage: www.elsevier.com/locate/jmarsys

Multiple controls on carbon dioxide sequestration in the beagle channel (Southern Patagonia) in early fall

Ludmila Caetano [a,b], Carles Guallar [c,d], Jacobo Martín [e,f], Montserrat Vidal [d], Leticia Cotrim da Cunha [g], Rosemary Vieira [a], Leonardo Amora-Nogueira [a,b], Josep L. Pelegrí [c], Humberto Marotta [a,b,*]

[a] Laboratory of Sedimentary and Environmental Processes (LAPSA-UFF), Department of Geography, Graduate Program in Geography, Universidade Federal Fluminense (UFF), Rio de Janeiro, Brazil
[b] Ecosystems and Global Change Laboratory (LEMG-UFF), Rede BrOA, Research Center on Biomass and Water Management (NAB-UFF), Graduate Program in Geosciences (Environmental Geochemistry), Universidade Federal Fluminense (UFF), Rio de Janeiro, Brazil
[c] Department of Physical and Technological Oceanography, Institut de Ciències del Mar, CSIC, Unidad Asociada ULPGC-CSIC, Barcelona, Spain
[d] Department of Evolutionary Biology, Ecology and Environmental Sciences, University of Barcelona, Barcelona, Spain
[e] Laboratorio de Oceanografía y Procesos Costeros, Centro Austral de Investigaciones Científicas (CADIC-CONICET), Ushuaia, Argentina
[f] CRG Marine Geosciences, Department of Earth and Ocean Dynamics, University of Barcelona, Barcelona, Spain
[g] Graduate Program in Oceanography, Faculty of Oceanography, State University of Rio de Janeiro, Rio de Janeiro, Rede BrOA, RedeClima/INPE, Brazil

ARTICLE INFO

Keywords:
pCO_2
High-resolution spatial variability
Patagonia
Sub-Antarctic waters
Beagle Channel

ABSTRACT

Subpolar coastal waters are key hotspots in the global carbon cycle. However, the small-scale distribution of partial pressure of carbon dioxide (pCO_2) in these environments and the physical and biological controls underlying this variability are still poorly understood. Here, we examine simultaneous high-resolution spatial measurements of wind speed and pCO_2, temperature, salinity, and in-vivo chlorophyll-*a* fluorescence (chl-*a* fluo, a proxy of phytoplankton biomass) in surface waters that were obtained during an oceanographic survey in the Argentinian Beagle Channel (subantarctic Atlantic Patagonian) in early fall 2017. The 240 km study transect (centered at 55°S - 67°W) was divided into two zones: (A1) The Beagle Channel innermost portion, semi-enclosed and subject to strong continental influence and (A2) its eastern outlet towards the open Southwest Atlantic. Discrete seawater samples were also collected for apparent oxygen utilization (AOU), nutrients and pH measurements. High-resolution spatial measurements revealed the persistence of pCO_2 below atmospheric equilibrium, increasing in median (interquartile range 25–75%) from 314 µatm in the inner Beagle Channel (A1) to 348 µatm towards the adjacent open sea (A2). A decrease in atmospheric CO_2 sequestration was associated with an increase in water temperature from 9.5 °C to 10.7 °C, salinity from 30.8 to 32.5, and chl-*a* fluo from 2.24 to 2.91 mg m^{-3} along the coastal-offshore gradient. Low AOU and nutrient levels were found in regions inside the channel. Indeed, the relationships between CO_2 and temperature or salinity were significantly different from those expected from the theoretical solubility effect, indicating a dominance of metabolic over physicochemical controls on this gas. Moreover, physical factors such as vertical stratification contributed to the variable surface pCO_2 values. These findings reveal the existence of short-scale spatial variability of CO_2 in the Beagle Channel, improving our understanding of the multiple controls on atmospheric carbon sequestration in extensive subpolar continental shelves.

1. Introduction

The ocean plays a critical role in global climate due to its capacity to incorporate atmospheric carbon dioxide (CO_2) through the chemical, biological and physical pumps, thus reducing the atmospheric concentration of this greenhouse gas (Stock et al., 2020). The ocean CO_2 sink has been estimated to withdraw about 25% of total carbon (C) emissions from anthropogenic sources during the last decade (Friedlingstein et al.,

* Corresponding author at: Laboratory of Sedimentary and Environmental Processes (LAPSA-UFF), Department of Geography, Graduate Program in Geography, Universidade Federal Fluminense (UFF), Rio de Janeiro, Brazil.
E-mail address: humbertomarotta@id.uff.br (H. Marotta).

https://doi.org/10.1016/j.jmarsys.2023.103858
Received 31 October 2021; Received in revised form 28 December 2022; Accepted 13 January 2023
Available online 16 January 2023

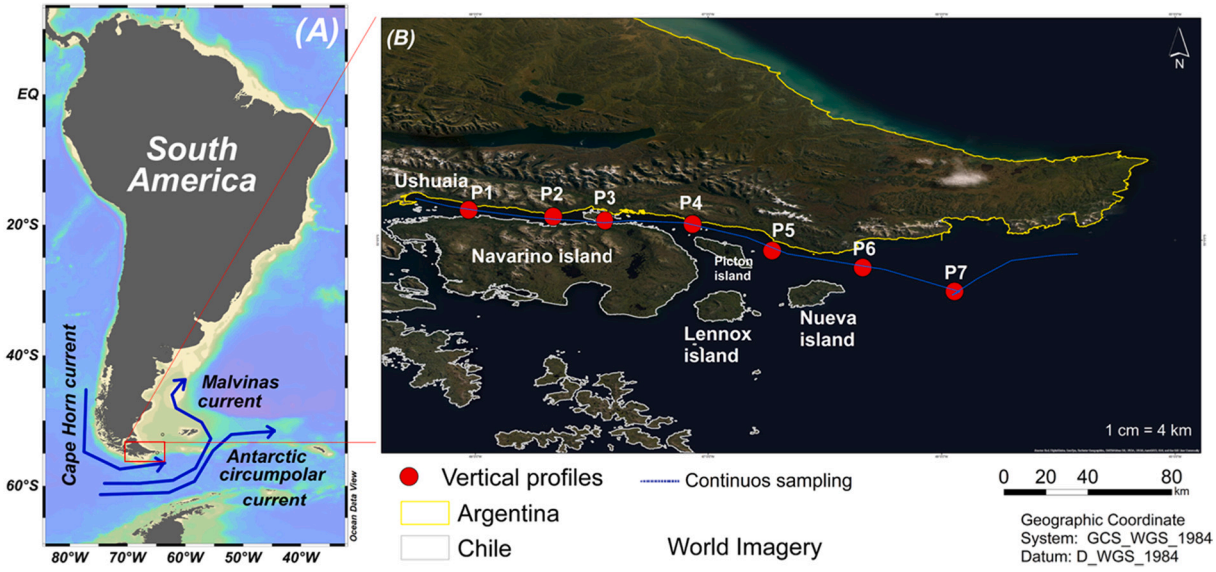

Fig. 1. Study area encompassing (A) a general view of South America and the schematic path of main marine currents (blue solid lines) at its southernmost end, and (B) a detailed region of the Beagle Channel and the adjacent sea. The red dots indicate the location of the sampling stations, while the blue line shows the cruise track with high-resolution spatial sampling of surface pCO_2 (μatm), salinity, temperature (°C), and chl-*a* fluo (mg m^{-3}). The map plots were created in Ocean Data View software (Schlitzer and Mieruch, 2021) ArcGIS. (For interpretation of the references to colour in this figure legend, the reader is referred to the web version of this article.)

2020). Despite their relatively small area, coastal waters exhibit higher and spatially variable net CO_2 uptake rates due to more intense physicochemical (e.g., the balance between dissolution and carbonation; Hoegh-Guldberg et al., 2007) and metabolic (e.g., the balance between biomass production and degradation; Breitburg et al., 2018) controls as compared to the open ocean. The coastal ocean CO_2 sink is very sensitive to continental freshwater inputs, as subsequent changes in temperature and salinity can affect both the marine carbonate system and the ecosystem metabolism (Cao et al., 2020), typically associated with changes in pH and the availability of organic substrates and nutrients (Borges et al., 2005; Libes, 2011). In oceanic waters, the dominant role of internal metabolism over physicochemical processes on CO_2 dynamics is indicated by their negative relationships with the apparent oxygen utilization (AOU) (Borges et al., 2005). Furthermore, the rates of C uptake in coastal waters may also be substantially altered by anthropogenic increases in temperature and nutrient inputs, given their impacts on physicochemical and metabolic processes (Guan et al., 2020).

High-latitude subpolar regions are known to show a marked seasonality of environmental variables and biological activity (Bianchi et al., 2005). Lower productivity and respiration rates increase nutrient availability under very cold conditions in winter, while increased light irradiance and temperature associated with terrestrial sources caused by melting during the warmer months support a stronger C pump and higher nutrient consumption by autotrophs (Gruber, 2014; Laruelle et al., 2018; Orselli et al., 2018). In southern South America, the intense phytoplankton blooms that take place from late spring to early fall in Patagonian coastal waters have been regarded as a major cause for lowering the sea surface partial pressure of CO_2 (pCO_2) below atmospheric equilibrium, causing a net annual C uptake (Schloss et al., 2007). At surface waters of the northern Antarctic Peninsula, biologically-mediated atmospheric CO_2 uptake is commonly observed in summer (Monteiro et al., 2020a), while net emissions are reported in winter due to low primary production in response to the decrease in temperature and the upwelling of CO_2–rich deep waters (Monteiro et al., 2020b).

Fjords are the deepest estuaries found at high latitudes, of glacial origin. They receive high seasonal inputs of meltwaters, carrying terrigenous biomass (Silva et al., 2011) and nutrients that support aquatic primary production (Jacob et al., 2014). These factors, associated with typically sluggish water circulation, contribute to a high net global accumulation of organic matter in fjords (Smith et al., 2015). Along the Patagonian coasts, subpolar estuaries stand out for their high biological productivity (Behrenfeld and Falkowski, 1997), acting as a considerable CO_2 sink (Bianchi et al., 2005, 2009; Kahl et al., 2017; Orselli et al., 2018) due to large phytoplankton blooms during spring (Bianchi et al., 2009; Garcia and Garcia, 2008).

The Beagle Channel, located at the southern end of Patagonia (Fig. 1), constitutes a unique subantarctic ecosystem influenced by freshwater inputs from seasonal melting and rainfall (Iturraspe et al., 1989), which contribute to significant vertical and zonal thermohaline gradients (Martin et al., 2019; Flores Melo et al., 2020). Dissolved and particulate organic compounds from multiple natural sources are delivered to this channel – including peat bogs, nearshore forests and numerous rivers and streams – adding to the autochthonous primary production by the marine phytoplankton (Almandoz et al., 2011; Barrera et al., 2017). Likewise, at certain spots like the city of Ushuaia, anthropogenic inputs must be taken into account (Amin et al., 2010). Previous evidence indicates that well-ventilated, macronutrient-rich oceanic Subantarctic Surface Water, that fills the inner basins of the Patagonian fjords and channels, shows variable O_2 and CO_2 saturation, especially due to the increased sequestration of atmospheric CO_2 by the biological productivity during the warm summer austral months (Torres et al., 2011, Torres et al., 2021). Despite the large extent and complex hydrodynamic properties of Patagonian fjords and channels, few studies have addressed the potentially important small-scale spatial variability of pCO_2 and its driving factors (Torres-Mellado et al., 2011). These few available studies have confirmed highly variable pCO_2 over short distances in subpolar coastal waters, indicating a complex interaction between physicochemical and metabolic processes that still need to be better understood in productive regions of the Southern Ocean (Caetano et al., 2020).

This study aims to assess pCO_2 and the factors controlling its spatial variability during early fall along a transect that runs along the Beagle Channel into the adjacent coastal sea (Argentinian Patagonia, South America), with substantial temperature and salinity gradients, using the first high-resolution measurements reported in the region. The study area and methods are presented in Section 2, the observations are shown

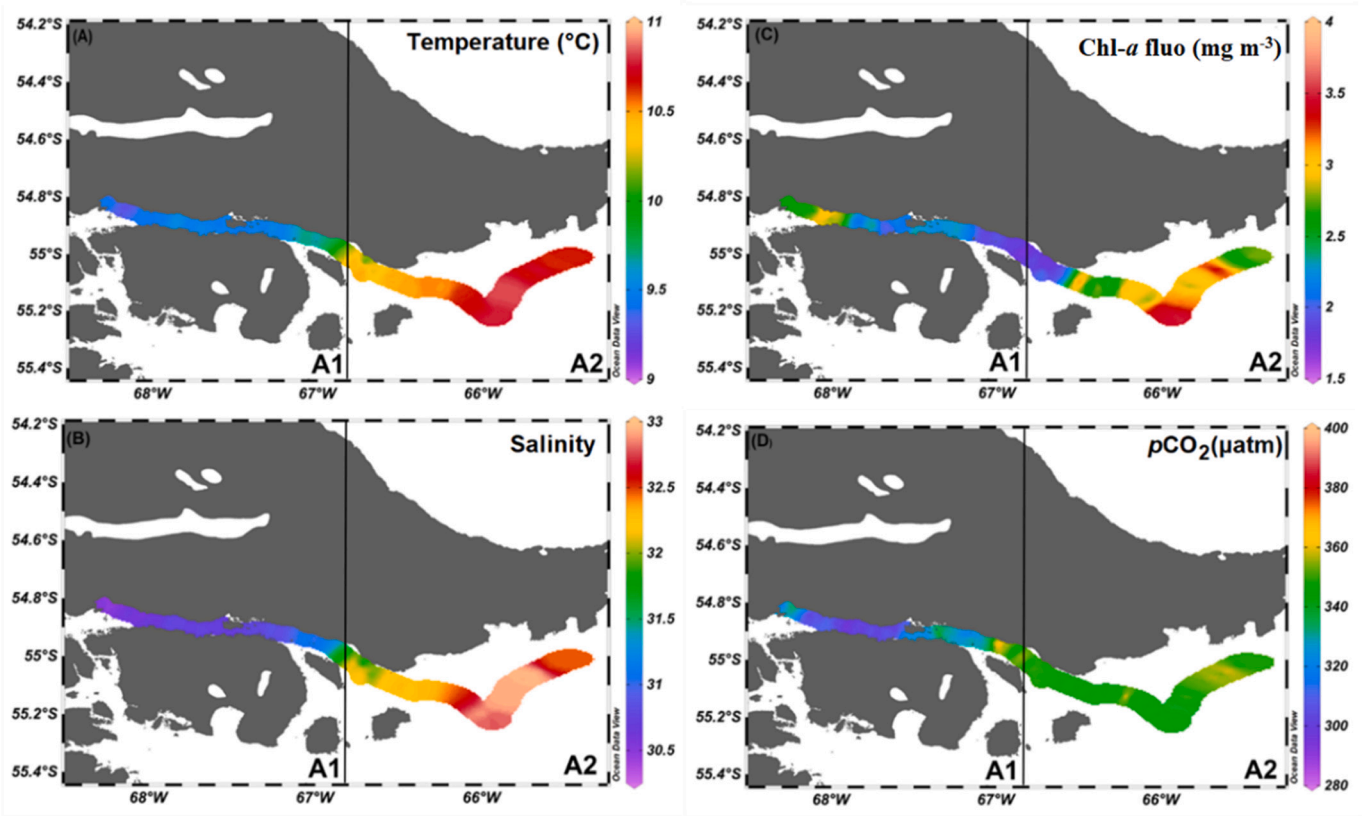

Fig. 2. Spatial distribution of (A) temperature (°C), (B) salinity, (C) chl-*a* fluo (mg m^{-3}), and (D) pCO_2 (µatm) in surface waters from the inner part of the Beagle Channel to the adjacent coastal sea, in fall 2017. The A1 and A2 zones are delimited by the meridian along 66°50′W. Images were created in Ocean Data View software (Schlitzer, 2021).

in Section 3 and the processes behind the observed variability are discussed in Section 4, closing with the conclusions in Section 5.

2. Materials and methods

2.1. Study area

The Patagonian region covers a vast area between the Pacific and Atlantic coasts in Southern South America, extending from about 39°S at the northern Colorado River to nearly 56°S at Cape Horn (Ramos, 2008; Saraceno et al., 2021). Along a jagged coastline shaped by a series of glacial valleys, fjords, islands and channels, the climate ranges from temperate in the north to cold-temperate in the south (Prohaska, 1976), and is influenced by local factors, especially the topography and the wind regime (Coronato, 1993). In the eastern part of Patagonia, the average annual air temperature ranges from some 12 °C in the northeast to about 3 °C in the south, while the absolute minimum temperatures are below −20 °C towards the southwest (Paruelo et al., 1995).

Precipitation over eastern Patagonia is mostly produced by disturbances embedded in the westerly winds, largely modified by the austral Andes. Uplift on the windward side leads to hyper-humid conditions along the Pacific coast and the western slope of the Andes; in contrast, downslope subsidence dries the eastern plains leading to arid, highly evaporative conditions (Garreaud et al., 2013). Hence, the high precipitation in the southern Pacific coast contributes to glacier and river formation at high altitudes. On the other hand, the very complex geomorphology displays a diverse and dense network of channels, embayments and fjords – shaped by the interplay of tectonic and glacial processes and sea-level fluctuations (De Muro et al., 2018) – that receive substantial and seasonal freshwater inputs from precipitation (Dávila et al., 2002). The Patagonian fjords and channels are typically characterized by a two-layer vertical structure composed of brackish water near the surface (5–10 m) and saltier homogeneous water at depth (Sievers and Silva, 2008).

As part of the Fuegian system of fjords and channels of the Magellan region in the southern end of South America (centered near 55°S and 69°W), the Beagle Channel is a succession of drowned glacial valleys that connects the Atlantic and Pacific oceans with an average width of near 5 km along a length of some 300 km (Bujalesky et al., 2004; Giesecke et al., 2021) (Fig. 1). The ancient valley, left behind by retreating glaciers after the last glacial maximum, was subsequently inundated by the sea about 10,000 BP, forming the present interoceanic conduit (Bujalesky, 2011; Björck et al., 2021). This East-West trending tectonic lineament was deeply carved by successive glacial cycles (Rabassa, 2008), resulting at present in a very irregular bathymetry, comprising an intricate succession of islands, embayments and micro-basins up to 400 m deep separated by steep sills as shallow as 20 m. The tidal regime is mixed semidiurnal and *meso*/microtidal (average 1.1 m and maximum 2.3 m) (D'Onofrio et al., 2016). The Beagle Channel waters belong to the subantarctic neritic domain (Hamamé and Antezana, 1999), which is mostly affected by the Pacific Ocean (Antezana, 1999). The general circulation is from west to east (Balestrini et al., 1998; Martin et al., 2019), with shallow sills at both the eastern and western boundaries that constrain the exchange between oceanic and inland waters (Giesecke et al., 2021).

The innermost zones of the Beagle Channel show a marked seasonally changing vertical structure, with a well-mixed water column in winter and a stratified column in spring and late fall, with its pycnocline located near 50–70 m (Flores Melo et al., 2020). The phytoplankton growth also shows a pronounced seasonality, between low biomass

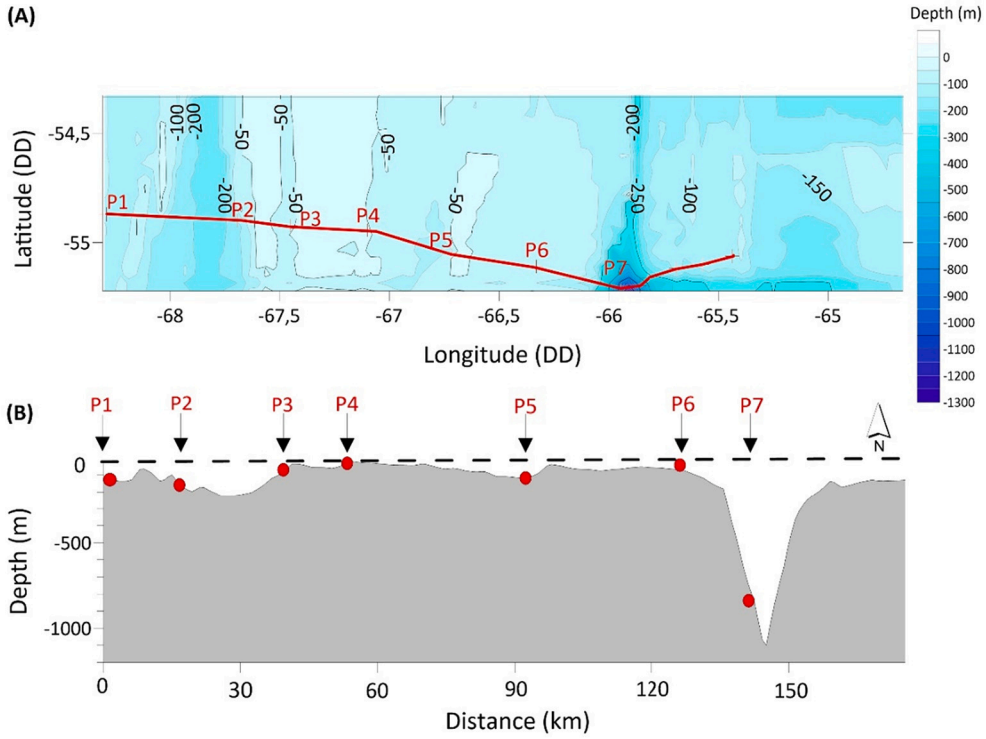

Fig. 3. Bathymetry along the Beagle Channel, showing (A) bathymetric contours and (B) the depth variations along the cruise track in the west-east direction. The red line in (A) indicates the sampling transect, while the red dots in (B) show the location of the seven sampling stations. The dashed line in (B) represents the sea level. The bathymetric profile was constructed using Surfer 21 (Golden Software, Colorado, USA; version 2021). (For interpretation of the references to colour in this figure legend, the reader is referred to the web version of this article.)

during fall-winter and massive increases during spring-summer, indicated by minimum surface values in winter (~0.1 μg C L^{-1}) and peak values in early spring (up to 141 μg C L^{-1}), respectively (Almandoz et al., 2019; Almandoz et al., 2011). Higher vertical summer stratification (i.e., warmer and fresher surface waters) together with more sluggish circulation (Cucco et al., 2022), increase the availability of plankton-derived organic matter, causing an increase in respiration that may cause oxygen depletion in bottom waters (Martin et al., 2016; Flores Melo et al., 2020).

2.2. Study design

The R/V Hesperides departed from Ushuaia on April 8, 2017 and followed a zonal transect (west-east direction) along the central portion of the Beagle Channel towards the SW Atlantic (Fig. 1), totalling 27 h of sampling over 240 km centered at (55°S, 67°W). Continuous high-resolution spatial measurements of pCO_2, temperature, salinity, and in-vivo chlorophyll-*a* fluorescence (chl-*a* fluo, a proxy of phytoplankton biomass) in surface seawater (at about 5 m depth) were coupled with simultaneous wind speed measurements at 1 min intervals aboard the ship. In addition, vertical profiles of water temperature, AOU, and chl-*a* fluo were conducted at 7 stations along the study transect (Fig. 1B) using a factory-calibrated SBE 911plus conductivity-temperature-depth (CTD) profiler. At each sampling station, discrete samples of marine surface waters were taken for analysis of dissolved inorganic nutrients (nitrite, nitrate, phosphorus and silicate), AOU and pH with a 12 L Niskin bottle system, while dissolved inorganic carbon (DIC) concentrations and air-sea CO_2 fluxes were estimated from physicochemical calculations (further details in the Analytical Methods section). To determine the relationship between pCO_2 and seawater properties at the sea surface, a principal component analysis (PCA) on the discrete sample data ($N = 7$) was performed. Then, based on the distribution of the sea surface parameters and the PCA clusters, the sampling area was divided into two zones from west to east: (A1) the inner Beagle Channel and (A2) the eastern Beagle sector into the adjacent Southwest Atlantic.

2.3. Analytical methods

2.3.1. pCO_2 in surface seawater

The pCO_2 in marine surface waters (down to about 5 m) was measured using an equilibrator (i.e., a Plexiglas tube with a diameter of 8 cm and height of 43 cm filled up with marbles) in a closed system with a non-dispersive infrared gas analyzer (EGM-4, PP-systems), keeping the internal pressure equal to atmospheric using a fine plastic tube (diameter of 3 mm) open to the atmosphere (Frankignoulle and Borges, 2001). This equilibrator-infrared analyzer system for determining pCO_2 in waters has been widely used onboard oceanographic ships (Butterworth and Miller, 2016; Delille et al., 2014). The water flows into the system showed a constant rate of 1–2 L min^{-1} from the top to the bottom, associated with an internal air mixing by another pump (Borges et al., 2006). The air from the equilibrator was still dried using a Drierite column before passing through the gas analyzer. The infrared gas analyzer was calibrated at the beginning and end of the sampling period with CO_2 standards of 106, 4,061,034, and 10,037 ppmv (Messer Americas), showing an uncertainty of ±2 ppmv in the studied range.

The sea surface pCO_2 (pCO_{2_sea}; μatm) was estimated from the pCO_{2_sea} at the temperature of equilibration (Teq), corrected by in situ temperature and salinity as described by.

The pCO_{2_sea} at T_{eq} (μatm) was calculated using Eq. (1):

$$pCO_{2\_}sea\left(T_{eq}\right) = Vco2eq\left(P_{atm} - P_{wat}\right) \quad (1)$$

where Vco2_eq is the mole fraction concentration (ppm) of CO_2 in the dried equilibrated carrier gas, and P_{atm} (atm) is the internal equilibration pressure, assumed to be equal to the atmospheric pressure; P_{wat} (atm) is the equilibrium water vapour pressure at the sea surface salinity, as determined by the ship's thermosalinograph, and T_{eq} (K), following Eq. (2):

$$P_{wat} = (1/760)\left(1–5.368\times10^{-4}\,S\right) exp.\left\{[0.0039476–(1/Teq)]/1.8752\times10^{-4}\right\} \quad (2)$$

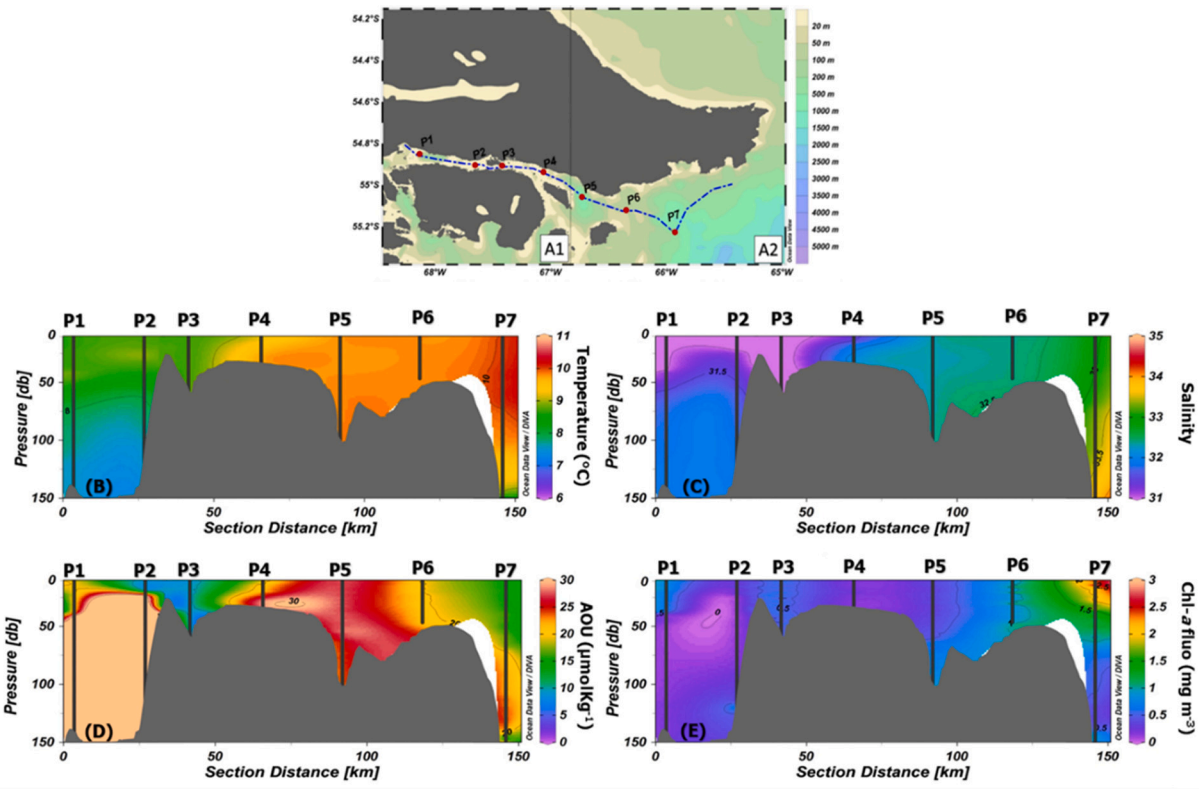

Fig. 4. (A) Map of the Beagle Channel with the position of the sampling stations. Hydrographic sections of (B) temperature (°C), (C) salinity (PSS-78), (D) AOU (µmol Kg^{-1}), and (E) chl-*a* fluo (mg m^{-3}) along the Beagle Channel. The location of the stations is drawn as vertical black lines, and the seafloor is indicated in grey colour, as obtained from the vessel echosounder and digitalization of the nautical chart H-477 (Argentinian Hydrographic Service). Blank spaces are areas of insufficient data from interpolation.

where S is the sea surface salinity (S; dimensionless) and Teq (K) as in Eq. (1).

Then, pCO_{2sea} was estimated using Eq. (3):

$$pCO_{2\,sea} = pCO_{2\,sea}\left(T_{eq}\right)\, exp\left[0.0423\ \left(T_{sea} - T_{eq}\right)\right] \quad (3)$$

where 0.0423 is the increase rate per °C (%) between in situ and equilibrator temperature and T_{sea} (K) is the sea surface temperature measured by the ship's thermosalinograph. The difference between T_{eq} and T_{sea} at the time of pCO_2 measurements varied from 0.5 to 0.8 °C, in the same range as reported by Takahashi et al. (1993).

2.3.2. Dissolved inorganic nutrients

Water samples were immediately filtered, through pre-combusted (450 °C, 4 h) 47 mm diameter glass fiber filters (Whatman GF/F, 0.7 µm nominal pore size) in an acid-cleaned glass filtration system, under low N_2-flow pressure. Filtered samples were kept frozen (−20 °C) in 30 mL polypropylene tubes for three months before analysis of nitrate, nitrite, and phosphate. Dissolved inorganic silicate concentrations were determined on non-filtered samples. The nutrient analysis was performed following the spectrophotometric determination methods reported in Grasshoff et al. (2009)) using an AA3 HR Seal Analytical instrument, showing a maximum uncertainty of 0.13, 0.20, 0.20, and 0.5% for the sum of nitrate and nitrite, nitrite, phosphate and dissolved silicate concentrations, respectively.

Table 1
Physicochemical variables of surface waters from discrete sampling, including pCO_2 (µatm), temperature (°C), salinity (practical scale PSS-78), chl-*a* fluo (mg m^{-3}), AOU (µmol Kg^{-1}), pH, nitrate (µM), nitrite (µM), silicate (µM) and phosphate (µM). *nd* = no data.

Variables	Sampling Stations						
	A1				A2		
	P1	P2	P3	P4	P5	P6	P7
pCO_2	333	327	329	351	348	347	379
Temperature	8.7	8.8	8.7	9.0	9.8	9.8	10.0
Salinity	30.9	30.9	30.8	31.3	32.3	32.4	32.9
Chl-*a* fluo	0.95	0.38	0.66	0.23	0.36	0.99	2.04
AOU	16.97	10	9.95	9.61	16.26	27.21	14.44
pH	7.9	*nd*	8.1	8.1	7.9	7.9	8.2
Nitrate (µM)	6.9	4.41	4.29	4.39	7.06	6.68	8.63
Nitrite(µM)	0.24	0.22	0.19	0.23	0.45	0.40	0.53
Silicate (µM)	1.26	0.83	0.83	1.12	1.80	1.14	1.20
Phosphate (µM)	0.83	0.79	0.73	0.79	1.04	0.85	0.85

2.3.3. pH and AOU

Water samples for pH were collected into 500 mL glass-stoppered bottles, which were fixed with 2.5 mL of a 1 g L^{-1} $HgCl_2$ solution (Grasshoff et al., 2009) to avoid biological activity of the samples until their analysis. During the calculations, the corresponding correction for the addition of the $HgCl_2$ solution in the samples is done.

pH was measured by a potentiometric glass electrode Metrohm Ecotrode plus using a Metrohm 888 Titrando equipped with 801 stirrer and controlled by Tiamo 2.5 software (Dickson et al., 2007). The system was periodically tested. For the pH electrode control, TRIS and AMP standard solutions prepared in the laboratory were used. The buffers were prepared in synthetic seawater according to Dickson et al. (2007). In addition, TRIS (batch 2) Certified Reference Materials (CRM), provided by Andrew Dickson's laboratory at the Scripps Institution of Oceanography, were also used to produce substandard materials for calibration. For this purpose, 50 L of seawater filtered with GF/F Whatman fiber filters were fixed with the $HgCl_2$ solution and stored in the laboratory. This substandard was daily analyzed for pH (mean and standard deviation of 7.946 and 0.05, respectively, representing 0.6% of variability through all the analyses). Once the analysis was done, the calculations procedure of Dickson et al. (2007) were applied to obtain pH.

In turn, AOU (μmol kg^{-1}) were estimated when quality-controlled in situ O_2 (μmol kg^{-1}), temperature (T, °C) and salinity (S) were all measured at the same geographic location, time, and depth. AOU is the difference between the equilibrium saturation concentration for in-situ physicochemical conditions and the respective measured dissolved oxygen concentration in waters (Weiss, 1974). This variable was calculated using the software Ocean Data View (version 5.6.3).

2.3.4. Vertical profiles

Vertical hydrographic profiles were obtained with a SeaBird 911 plus CTD profiler, equipped with dual temperature and conductivity sensors to detect any potential drift. Primary oceanographic variables were used to compute derived (salinity, density) variables by means of the SBE Data Processing Package (v. 7.26.7). The CTD was also equipped with a chl-*a* fluo sensor, calibrated with measurements of discrete water samples by fluorometry (Yentsch and Menzel, 1963) in a Turner-Designs fluorimeter ($r^2 = 0.88$, p-v < 0.001, $n = 22$), and two dissolved oxygen (DO) sensors, calibrated with measurements of discrete surface water samples ($N = 300$) using the Winkler titration method (Dickson et al., 2007). The correction factor for the DO sensors applied is 1.0746, with no temporal or spatial significant dependences (Orúe-Echevarría et al., 2020).

2.3.5. Determination of CO_2 concentrations in seawater and its physical-chemical and biological controls

The CO_2 concentrations observed at the sea surface (CO_2-obs; μmol L^{-1}) were determined by Henry's law (Cole and Caraco, 1998):

$$CO_{2obs} = pCO_{2sea}\, K_h \tag{4}$$

where pCO_{2sea} (μatm^{-1}) is estimated as in section 2.1.1 and K_h is the Henry's solubility constant for CO_2 at sea surface temperature and salinity (mol L^{-1} atm^{-1}).

The Kh (mol L^{-1} atm^{-1}) was calculated as follows (Weiss, 1974)

$$ln(\mathrm{Kh}) = A_1 + A_2(0.01\mathrm{T}) + A_3 ln(0.01\mathrm{T}) + \mathrm{S}[B_1 + B_2(0.01\mathrm{T}) + B_3(0.01\mathrm{T})2] \tag{5}$$

where T (K) and S (dimensionless) here refer to the sea surface layer. The other dimensionless constants are $A_1 = -58.0931$, $A_2 = 90.5069$, $A_3 = 22.2940$, $B_1 = 0.027766$, $B_2 = -0.025888$ and $B_3 = 0.0050578$.

In turn, the CO_2 concentrations of water at equilibrium with the overlying atmosphere, over the range of in situ observed sea surface temperature and salinity (CO_{2_exp}; μmol L^{-1}), were calculated from Henry's law and the fugacity pressure relationship as follows (Weiss, 1974)

$$\left[CO_{2\_exp}\right] = pCO_{2\_atm}(K_h\ exp\ ((1 - P_{atm})\ Vco2/(R\ T)))$$

where pCO_{2_atm} (μatm) is the pCO_2 in equilibrium with the overlying atmosphere pressure; this value is obtained from the Ushuaia coastal station located in the margin of the Beagle Channel (401.65 μatm in April 2017). data available at *https://gml.noaa.gov/aftp/data/trace_gases/co2/flask/surface/txt/co2_ush_surface-flask_1_ccgg_month.txt*), which were similar to the in-situ measurements without the influence from the ship chimney during the sampling period.; Vco2 is the

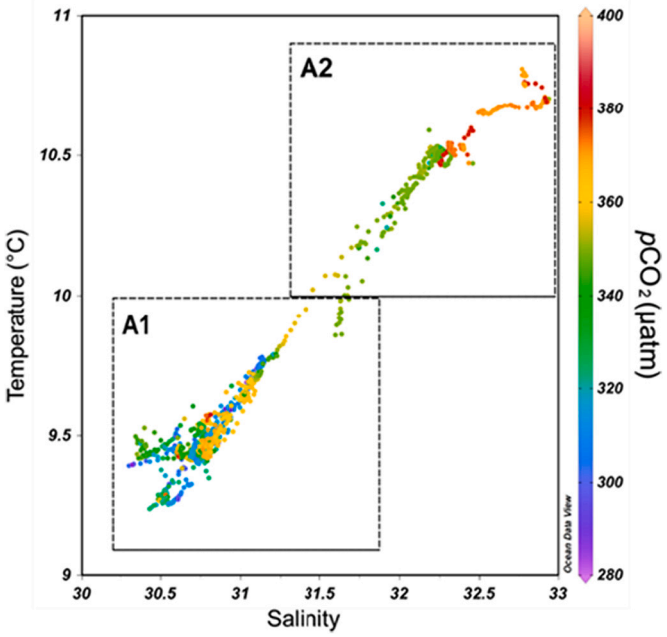

Fig. 5. Temperature versus salinity diagram, coloured for pCO_2 (μatm). Graphs were created in Ocean Data View software (Schlitzer, 2021).

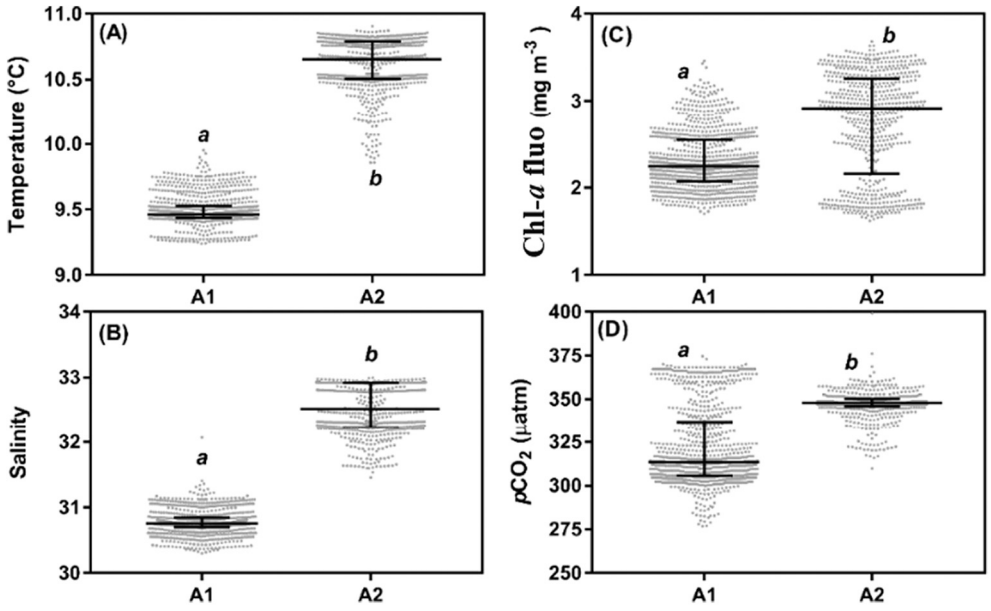

Fig. 6. Comparison between zones A1 and A2: (A) temperature (°C), (B) salinity, (C) chl-*a* fluo (mg m^{-3}), and (D) pCO_2 (µatm) in surface waters. Each grey dot represents one measurement along the transect ($N = 903$ in A1 and $N = 629$ in A2 for all variables). Horizontal lines and vertical bars show the median and 25–75% interquartile range, respectively. Different letters (a and b) in each panel represent significant differences (Mann Whitney test; $p < 0.05$).

partial molar volume of dissolved CO_2 (ca. 32×10^{-3} L mol^{-1}) and R is the ideal gas constant (ca. 0.082 L atm K^{-1} mol^{-1}).

In the absence of physical mixing and metabolic control, variations in temperature and salinity determine the expected changes in ocean CO_2 caused by the solubility of this gas in water (Takahashi et al., 1993). Then, the expected CO_2 variations caused solely by physicochemical processes (CO_{2_exp}) over the observed range of sea surface temperatures (i.e., assuming a constant salinity as the observed median) and salinities (i.e., assuming a constant temperature as the observed median °C) were compared with the actual relationships between the observed CO_2 (CO_{2_obs}) and the seawater temperature or salinity. Low deviations between observed and expected models indicate that the effects of solubility could be dominant on sea pCO_2, while higher differences indicate the prevalence of biological over physical-chemical control (Jiang et al., 2008; Joesoef et al., 2015).

2.3.6. *Air-sea CO_2 exchange*

The air-sea CO_2 flux (FCO_2; mmol m^{-2} d^{-1}) was estimated as follows:

$$FCO_2 = k\, K_h\, (\Delta pCO_2)_{sea-atm} \quad (7)$$

where $(\Delta pCO_2)_{sea\text{-}atm}$ is the difference between the observed pCO_2 observed in sea surface waters (pCO_{2_sea}) and equilibrium pCO_2 value with the overlying atmosphere (pCO_{2_atm}) (see Sections 2.1.1 and 2.1.5, respectively). Finally, k is the CO_2 transfer velocity (cm h^{-1}) as parametrized next (Wanninkhof, 2014):

$$k = C\, U^2\, (Sc/660)^{-0.5} \quad (8)$$

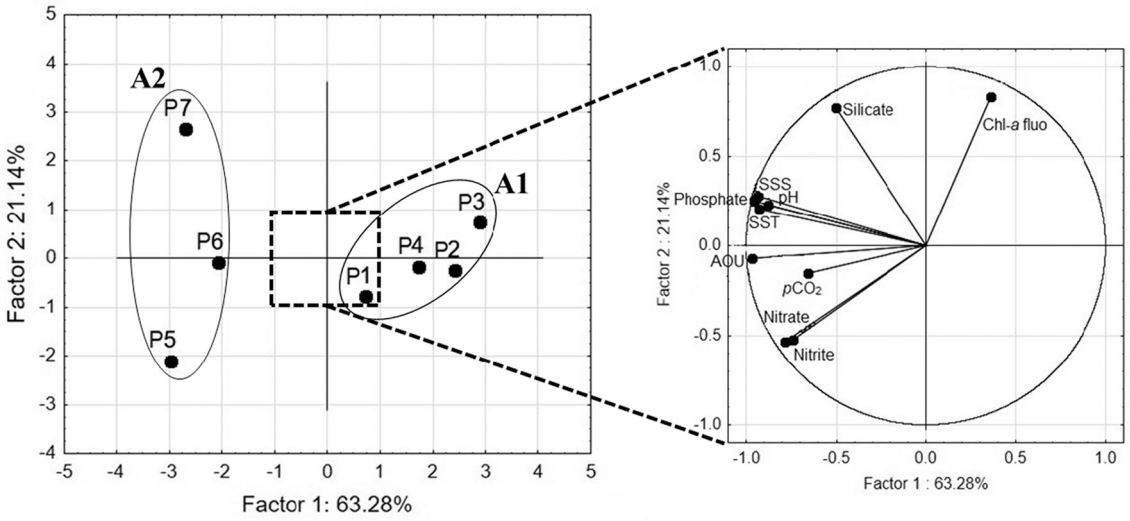

Fig. 7. Principal components analyses (PCA) for surface water data in the inner part of the Beagle Channel (region A1 with stations P1, P2, P3, and P4) and its adjacent sea (region A2 with stations P5, P6, and P7).

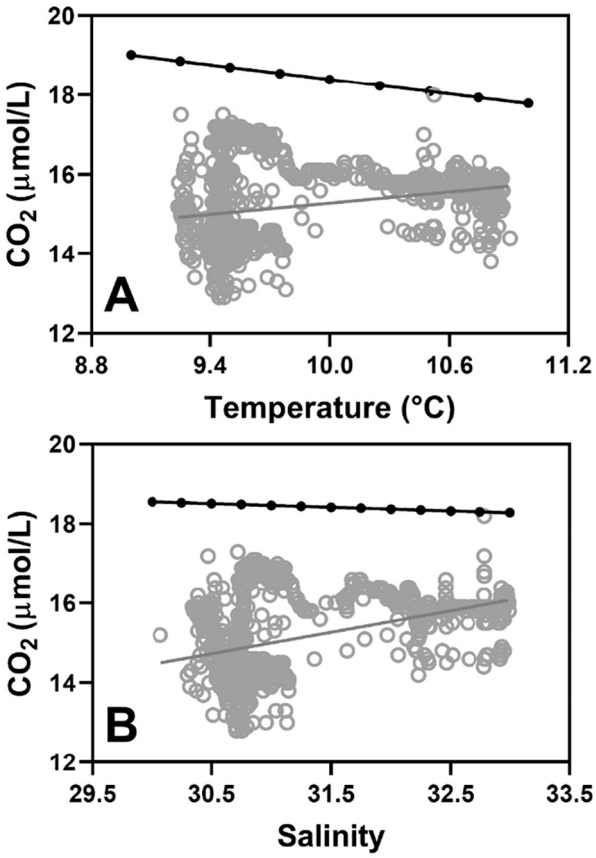

Fig. 8. CO_2 concentration (µ mol L^{-1}) as expected from the solubility effect (black dots) and as determined from the pCO_2 observations (grey circles), plotted as a function of the observed (A) salinity and (B) temperature (°C) in surface waters. The data comes from the entire study area. The black solid lines represent the linear relation for the expected CO_2 in each panel (A) CO_2-exp = 0.61 T + 24.52 (R^2: 1.0; $p < 0.05$) and (B) CO_2-exp = −0.09 S + 21.31 (R^2: 1.0; $p < 0.05$). The grey solid lines represent the linear fit to the CO_2 observations, (A) CO_2-obs = −0.47 T + 10.60 (R^2: 0.09; $p < 0.05$) and (B) CO_2-obs = −0.54 S + 1.67 (R^2: 0.24; $p < 0.05$). The slopes of CO_2-exp and CO_2-obs are significantly different (ANCOVA, $p < 0.05$) in both (A) and (B).

where C = 0.251 (cm h^{-1}) (m s^{-1}) $^{-2}$, U is the in-situ wind speed (m s^{-1}) at 10 m above ground, and *Sc* is the Schmidt number (dimensionless).

2.4. Statistical analysis

The transformed data did not meet the assumptions of normal distribution (D'Agostino & Person test) and homogeneity of standard deviations (Bartlet test, $p > 0.05$) (Zar, 2010). Thus, the non-parametric Mann-Whitney test was applied to assess significant differences ($p < 0.05$) of high-resolution spatial variables (pCO_2, salinity, temperature and chl-*a* fluo) between both study zones A1 and A2. Further, the relationships between sea surface pCO_2 and the physicochemical variables (dissolved nutrient concentrations, pH, AOU and TA) in the water samples were assessed using a principal component analysis (PCA). With the purpose that all variables be considered equally scaled, and hence analyzed on the basis of correlations rather than covariances, data were normalized by autoscaling for PCA (Parente and Sutherland, 2013). Statistical analyses and graphs were performed using GraphPad Prism software (GraphPad Prism Software Inc., San Diego, USA; version 7.0), except the PCA that used the Statistica software (StatSoft Inc., Tulsa, USA; version 7.0).

3. Results

Continuous high-resolution measurements indicated a thermohaline zonal gradient in surface waters along the transect, from the central Beagle Channel towards the adjacent SW Atlantic Ocean (Fig. 2). Briefly, the inner part of the Beagle Channel presents a micro-basin about 235 m deep, followed in an eastward's direction by a major topographic constriction at Mackinlay Strait where the channel width shrinks from some 5 km to only 1.5 km and the bottom depth decreases abruptly from over 100 m to about 15 m. Further east and beyond Picton Island, the bottom depth increases largely from an average depth of 50 m to >1000 m as the channel opens to the adjacent continental slope (Fig. 3). For a more detailed description of the underwater features the reader is redirected to Bujalesky (2011) and Giesecke et al. (2021).

The vertical hydrographic profiles showed thermohaline stratification in some of the deepest Beagle Channel stations (P1 and P2, with 137 m and 150 m depth, respectively, and the seaward P7 with 874 m depth), but not in the station near the confluence of zones A1 and A2 (P5 with 137 m depth; Fig. 4). Indeed, an oxycline was observed in the deepest innermost stations of Beagle Channel (P1 and P2), but not in the station closest to the sea (P7; Fig. 4). Discrete samples of surface waters showed an overall increase in AOU with increasing temperature and salinity from the stations of zone A1 (P1, P2, P3 and P4) to A2 (P5, P6 and P7), while higher chl-*a* fluo was observed in the adjacent open sea, especially at P7 (Fig. 4). Surface waters of this outermost station still had the highest pH values and nitrate/nitrite concentrations, while the silicate and phosphate concentrations were slightly below the maximum values found in P5 (Table 1).

Furthermore, the relatively sharp change in sea surface temperature (SST) and salinity (SSS) as well as pCO_2 defined a boundary with l data in the gradient between an innermost shallow zone (A1) and an outermost deepest zone (A2; Fig. 5) around Picton Island. Spatial variations of temperature from 9.2 °C to 9.9 °C and salinity from 30.3 to 32.0 in A1 contrasted with the warmer (9.9–10.9 °C) and saltier (31.5–32.9) range

in A2, reflecting the influence of different surface water masses, namely modified Subantarctic Water and different sub-types of the so-called Estuarine Waters as defined by Silva et al. (1998).

Higher median temperature, salinity, chl-*a* fluo and pCO_2 values (increases by 11, 13, 6, and 32%, respectively) were observed in the adjacent sea (A2) as compared to zone A1 (Fig. 6). Median values (25–75% interquartile range) of pCO_2 varied from 313 (305–337) to 348 (346–350) μatm, temperature from 9.5 (9.4–9.5) °C to 10.7 (10.5–10.8) °C, salinity from 30.7 (30.7–30.8) to 32.5 (32.2–32.9), and chl-*a* fluo from 2.24 (2.08–2.55) to 2.92 (2.16–3.26) mg m^{-3} between A1 and A2 (Mann Whitney test; $p < 0.05$; Fig. 4). Despite this variability, the maximum pCO_2 value observed in surface waters in the study area (399 μatm in zone A2; Fig. 6) remained below the equilibrium value with the overlying atmosphere (401.7 μatm as detailed in the Methods section). Thus, the atmospheric CO_2 uptake by waters of Beagle Channel and adjacent sea during early fall was estimated to reach median values of 0.7 and 1.2 mmol m^{-2} d^{-1} for zones A1 and A2, respectively, contributing to an overall median influx of 0.9 mmol m^{-2} d^{-1} for the entire study area.

The marked differences in pCO_2 and other biological and physicochemical variables between zones A1 and A2 were also confirmed by the PCA, using all discrete surface-water data from the seven sampling stations. This multivariate analysis identified two groups, dividing the innermost stations of the Beagle Channel (P1, P2, P3 and P4 in A1) from those in the adjacent sea (P5, P6 and P7 in A2; Fig. 7).

Zone A1 was more related to chl-*a* fluo, while A2 to AOU, pCO_2, salinity, temperature, and nutrients, confirming that the seaward waters were warmer, saltier, more eutrophic, and had both higher AOU and pCO_2. According to the PCA analysis, factor 1 (pCO_2) was responsible for 63.3% of the total variance and factor 2 (SST) for 21.1%, so that both variables explained as 84.4% of the observed variability (Fig. 7). Overall, pCO_2 was affected positively by temperature, salinity, nutrients, and AOU. In addition, a negatively relationship between chl-*a* fluo and saltier waters was indicated by factor 2.

Finally, the observed concentrations of surface CO_2 along the studied transect showed significant positive relationships with temperature and salinity (linear regression, $p < 0.05$; Fig. 8). These positive slopes differ substantially from those negative values that would be expected due to decreased solubility with increasing temperature (−0.61 vs +0.47) and salinity (−0.09 vs +0.54; ANCOVA, $p < 0.05$) (Zar, 2010).

4. Discussion

4.1. High-resolution spatial variations in surface waters

The high-resolution distribution of pCO_2 along the entire transect from the innermost part of the Beagle Channel (A1) to the adjacent coastal sea (A2) during early fall reveals the role of multiple spatial controls, associated with the persistence of undersaturation and subsequent net sink of this gas at the sea-air interface. The surface pCO_2, chl-*a* fluo (a proxy of phytoplankton biomass), and thermohaline conditions showed substantial variations along this transect. The A1 zone showed lower salinity and temperature in surface waters likely due to increased freshwater input as compared to A2 in the seaward side. During the winter months, there is a reduction of the ecosystem metabolism because of the reduced insolation that leads to high nutrient availability, which is critical to support seasonal phytoplankton blooms in subsequent periods with higher solar radiation (Boyd, 2002). Previous work has demonstrated that Patagonian coast waters at the Southwest Atlantic (e.g., near the Beagle Channel) act as CO_2 sink, whereas northern areas act as a source likely due to upward flux of CO_2-enriched subsurface waters and the role of aquatic respiration (Bianchi et al., 2009). Thus, our results support the idea that upwelling-free fjords (Torres et al., 2011, Torres et al., 2021) and coastal sea (Schloss et al., 2007) in this region can be important CO_2 sinks maintained by high seasonal primary production.

4.2. Hydrographic gradients and the influence of geomorphological features

The bathymetric contrasts along the oceanographic transect may pose restrictions to the water flow along the channel and hence influence zonal gradients in seawater properties (Giesecke et al., 2021) and water residence times (Cucco et al., 2022). In particular, the topographic sill at Mackinlay Strait (minimum depth about 15 m) has been signalled in the past as a physical barrier that imposes different physical and biological properties to the east and west (e.g. Diez et al., 2018; Martin et al., 2019; Presta et al., 2022). However, according to the near-surface thermohaline signature recorded by the continuous system in our study (Fig. 2), this hydrographic front is shifted further east, discriminating between an inner (A1) domain strongly influenced by continental inputs and an outer (A2) domain more subject to oceanic influence.

In high-latitude ecosystems such as the fjords and estuaries along the Patagonian coasts, high precipitation and ice melting during warm periods induce lower sea surface salinity, contributing to vertical stratification through the formation of a halocline, an effect that can be reinforced through thermal stratification as the air temperature increases in the summer months (Dávila et al., 2002; Rignot et al., 2003). Such seasonal pattern has also been observed in the inner Beagle Channel, where vertical density stratification builds up in spring/summer and persists through autumn (Flores Melo et al., 2020; Martin et al., 2019). As a consequence of stratification, vertical mixing gets reduced and primary production decreases, also leading to the isolation of the CO_2-enriched waters below the pycnocline (Ahmed et al., 2020; Torres et al., 2011). Here, we found thermohaline vertical stratification in the inner stations of the Beagle Channel (stations P1 and P2), with important freshwater inputs from rivers and direct runoff to the surface layers (Iturraspe et al., 1989), as well as in the seaward extreme of the Chanel (station P7), with the bottom intrusion of relatively warm and salty ocean water masses. In contrast, vertically unstratified waters were observed between stations P4 and P6, located east of the marked narrowing of the Beagle Channel, from 4.5 to 6.5 to 1.5–2.0 km near station P3 (adjacent to the Tierras del Fuego Island). This result points to the role of either channel constrictions or seafloor topography controlling the hydrodynamics and water mixing in this region (Martin et al., 2019).

Furthermore, the inner stations of the Beagle channel also showed an oxycline associated with the pycnocline, which is caused by both thermal and haline stratifications, together with a slight decrease in chl-*a* fluo with depth. Previous evidence suggests that the vertical attenuation of light leads to a decrease in phytoplankton production with depth (Almandoz et al., 2019), and the lack of vertical mixing constrains the biological O_2 release and CO_2 pump to the photic layers above the pycnocline (Thomas et al., 2004). In this way, the AOU was generally higher in deep than surface waters along the vertical profiles, showing greater differences in inner regions of the Beagle Channel more influenced by the outflow from the catchment. Decreased oxygen levels, as found towards the bottom here, are typically caused by increased biological degradation of organic matter in coastal waters receiving greater terrestrial biomass inputs (Marotta et al., 2012).

4.3. Metabolic and physicochemical controls on sea surface CO_2

Our findings provide new insights into the drivers of atmospheric CO_2 removal in spatially variable subpolar coastal waters during early fall. Lower pCO_2 values and dissolved nutrient concentrations at two of the innermost sampling stations of the Beagle Channel (P2 and P3) could be attributed to the intense autotrophic activity after the spring peak (Amin et al., 2010; Almandoz et al., 2011). In turn, slightly higher salinity and pH in surface waters in the outermost station (P7) could be due to the decrease of acid freshwaters towards the open ocean (Cai et al., 2010).

Increased runoff caused by precipitation in the western side of the Patagonian Andes (Smith and Evans, 2007) and glacier melting

contribute to the inputs of continental freshwaters enriched in a wide variety of limiting nutrients in the Southern Ocean (Smetacek et al., 2012; Barrera et al., 2017). In addition to N and P, the terrestrial sources of silicic acid (Gonzalez et al., 2010) and dissolved iron (Gaiero et al., 2003; Garzón-Cardona et al., 2016) can enhance the uptake of CO_2 by phytoplankton in the fresher surface waters along the Patagonian coast. However, lower CO_2 undersaturation in the outermost sampling station (P7), which points at a relatively weak atmospheric CO_2 sink, contrasted with the observed high peaks of chl-*a* fluo. This appears contradictory, as phytoplankton biomass typically shows a negative rather than a positive relationship with pCO_2 (Carvalho et al., 2020), especially in the photic zone of the Austral coastal ocean (Monteiro et al., 2020b). In line with this, the proxies of phytoplankton biomass (i.e., chl-*a* fluo) and net oxygen consumption (i.e., AOU) did not show a negative relationship in the PCA analysis for the study surface waters, also contrasting with the typical pattern of high algal chl-*a* and low AOU reported in highly productive seawaters (Erickson and Thompson, 2018). A potential explanation is that more eutrophic conditions can support both increased primary production and net heterotrophic state at the sea surface worldwide (Duarte et al., 1998), including subpolar coastal surface waters (Conley et al., 2007). Moreover, the physical control of vertical stratification together with low-chlorophyll water inputs from ice melting may dilute the phytoplankton near-surface concentration (Schwarz and Schodlok, 2009), hence decoupling the chl-*a* concentrations from the autotrophic production and enhancing CO_2 removal with no observable algal biomass increase (Biddle et al., 2015).

As a result of the above processes, the observed CO_2 concentrations in surface waters were below the atmospheric equilibrium and positively related to temperature and salinity, instead of negatively related due to the solubility effect. This indicates the dominant role of metabolic rather than physicochemical controls in the Beagle Channel and its adjacent sea during early fall. This agrees with earlier reports for productive subpolar coastal waters (Caetano et al., 2020; Iriarte, 2018), which have been shown to play an important CO_2 sink worldwide (Takahashi et al., 2002). The biological controls were also indicated by the PCA results in the surface pCO_2 (factor 1) along the transect. Regarding the SST (factor 2), the small variation from P1 to P4 may be attributed to a high influence of ice melting in zone A1 and the high horizontal thermal gradient between the eastern Beagle channel (station P5) and the adjacent sea (station P7). Hence, the dissimilar vertical stratification, related to basin geomorphology and cold-water input from glacier melting, could also explain these differences between zones A1 and A2. Indeed, high nutrient concentrations towards the open ocean (i.e., warmer and more saline waters than in the inner channel) were positively related to both pCO_2 and AOU. The fjord waters show intense biological sink of atmospheric CO_2 followed by nutrient depletion due to phytoplankton uptake during the warm season (Torres et al., 2011), supporting the role of net autotrophy reducing CO_2 in the coastal sea of Southern Patagonia (Schloss et al., 2007).

4.4. Sea-air CO_2 fluxes

The Patagonian coastal waters have been described as an atmospheric CO_2 sink during the warm summer months due to autotrophic activity, although this is potentially reduced or even reversed during winter (Torres et al., 2011; Vergara-Jara et al., 2019). In contrast to the persistent CO_2 sink observed in this study (0.9 mmol m^{-2} d^{-1}), previous surveys in the surface coastal waters in Northern Patagonia during the fall indicated a net CO_2 emission of 6.5 mmol m^{-2} d^{-1} (Vergara-Jara et al., 2019). This difference may be attributed to the higher inputs of terrestrial organic matter that drive heterotrophy northward, likely related to the relatively warm annual conditions of the north temperate forests, located some 1500 km away from the subpolar vegetation around Beagle Channel (Olson et al., 2001). In addition, both CO_2 sink (Álvarez et al., 2002) and CO_2 source (Kerr et al., 2017), indicative of shifts between net autotrophy and heterotrophy, respectively, have been found in the subpolar coastal waters of the northern Antarctic Peninsula during the fall season.

Our early-fall estimates of atmospheric CO_2 uptake in the surface waters of the Beagle Channel, between its innermost portion and the adjacent sea, are in median ~ 75 and 60% lower than previously reported values for the Patagonian continental shelf sea during this season (Bianchi et al., 2009). Low CO_2 influx in marine waters has been attributed to the high contribution of organic substrates (Anderson et al., 2009), which has been confirmed in subpolar coastal waters (Kerr et al., 2017). A fjord-like bay situated in the South Shetland Islands (950 km south of the Beagle Channel) reaches much higher atmospheric CO_2 sink during late spring than reported here, between five (Ito et al., 2017) and 12 (Caetano et al., 2020) times higher. Although we are comparing different subpolar coastal waters, this may indicate that the net autotrophy diminishes during the warm summer period because of a decrease in nutrient availability (Torres et al., 2011; Torres et al., 2021).

5. Conclusions

The atmospheric CO_2 uptake in the Beagle Channel and the adjacent sea during early fall is estimated at 0.7 and 1.2 mmol m^{-2} d^{-1} for zones A1 (innermost Beagle Channel) and A2 (adjacent Southwest Atlantic Ocean), respectively, contributing to an overall average influx of 0.9 mmol m^{-2} d^{-1} for the entire study area. Furthermore, this study reveals a highly spatially variable atmospheric CO_2 sink that is modulated by multiple spatial controls, with a predominance of metabolic (i.e., the balance between biomass production and degradation) over physicochemical (i.e., solubility effect) processes. Furthermore, abrupt variations in seafloor topography and coastline morphology must be considered as physical controls on the surface pCO_2 via changes in vertical and horizontal mixing.

The substantial spatial variability of pCO_2 along the Beagle Channel during early fall is associated with higher CO_2 uptake in inner regions of the Beagle Channel, where lower salinity and temperature are conditioned by the freshwater inputs from glacier melting, as compared with the eastern opening of the channel to the coastal waters. This study contributes to a better understanding of the strong sensitivity of multiple biological, physical, and chemical controls on the short-scale spatial variability in subantarctic waters. This is particularly relevant because of the recognized central role of the Southern Ocean as a major global sink of CO_2.

Declaration of Competing Interest

The authors declare that they have no known competing financial interests or personal relationships that could have appeared to influence the work reported in this paper.

Data availability

Data will be made available on request.

Acknowledgements

We acknowledge support from the Spanish Government through grants CTM2014-56987-P (VA-DE-RETRO Project) and RTI2018-100844-B-C33 (SAGA project) and also recognize the institutional support of the Spanish Government through the Severo Ochoa Centre of Excellence accreditation (CEX2019-000928-S). This study was funded by grants from the Council for Research and Scientific Development of Brazil (CNPq, 203366/2019-0, 314995/2020-0) and the Research Support Foundation of the State of Rio de Janeiro (E-26/211.329/2021 and E-26/201.118/2022). H.M. and L.C.C. were awarded by CNPq Research Productivity and FAPERJ Scientist of Our State fellowships. L.C.C. was awarded by UERJ/PROCIENCIA fellowship. We warmly thank Dr. Gustavo Lovrich from CADIC-CONICET for a very generous donation

that made the navigation along the Beagle Channel possible.

References

Ahmed, M.M.M., Else, B.G.T., Capelle, D., Miller, L.A., Papakyriakou, T., 2020. Underestimation of surface pCO_2 and air-sea CO_2 fluxes due to freshwater stratification in an Arctic shelf sea, Hudson Bay. Elem. Sci. Anthr. 8 https://doi.org/10.1525/elementa.084.

Almandoz, G.O., Hernando, M.P., Ferreyra, G.A., Schloss, I.R., Ferrario, M.E., 2011. Seasonal phytoplankton dynamics in extreme southern South America (Beagle Channel, Argentina). J. Sea Res. 66, 47–57. https://doi.org/10.1016/j.seares.2011.03.005.

Almandoz, G.O., Cefarelli, A.O., Diodato, S., Montoya, N.G., Benavides, H.R., Carignan, M., Hernando, M., Fabro, E., Metfies, K., Lundholm, N., Schloss, I.R., Álvarez, M., Ferrario, M.E., 2019. Harmful phytoplankton in the Beagle Channel (South America) as a potential threat to aquaculture activities. Mar. Pollut. Bull. 145, 105–117. https://doi.org/10.1016/j.marpolbul.2019.05.026.

Álvarez, M., Rios, A.F., Roson, G., Rios, A.F., Roson, G., 2002. Spatio-temporal variability of air-sea fluxes of carbon dioxide and oxygen in the Bransfield and Gerlache Straits during Austral summer 1995-96. Deep Res. Part II Top. Stud. Oceanogr. 49, 643–662. https://doi.org/10.1016/S0967-0645(01)00116-3.

Amin, O., Comoglio, L., Spetter, C., Duarte, C., Asteasuain, R., Freije, R.H., Marcovecchio, J., 2010. Assessment of land influence on a high-latitude marine coastal system: Tierra del Fuego, southernmost Argentina. Environ. Monit. Assess. 175, 63–73. https://doi.org/10.1007/s10661-010-1493-5.

Anderson, L.G., Jutterström, S., Hjalmarsson, S., Wåhlström, I., Semiletov, I.P., 2009. Out-gassing of CO_2 from Siberian Shelf seas by terrestrial organic matter decomposition. Geophys. Res. Lett. 36 https://doi.org/10.1029/2009GL040046.

Antezana, T., 1999. Plankton of southern Chilean fjords: trends and linkages. Sci. Mar. 63, 69–80. https://doi.org/10.3989/scimar.1999.63s169.

Balestrini, C., Manzella, G., Lovrich, G., 1998. Simulación de Corrientes en el Canal Beagle y Bahia Ushuaia, Mediante un Modelo Bidimensional. Serv. Hidrogr. Nav. 98, 1–58. https://doi.org/10.13140/RG.2.1.1196.2729.

Barrera, F., Lara, R.J., Krock, B., Garzón-Cardona, J.E., Fabro, E., Koch, B.P., 2017. Factors influencing the characteristics and distribution or surface organic matter in the Pacific-Atlantic connection. J. Mar. Syst. 175, 36–45. https://doi.org/10.1016/j.jmarsys.2017.07.004.

Behrenfeld, M.J., Falkowski, P.G., 1997. Photosynthetic rates derived from satellite-based chlorophyll concentration. Limnol. Oceanogr. 42, 1–20.

Bianchi, A.A., Bianucci, L., Piola, A.R., Pino, D.R., Schloss, I., Poisson, A., Balestrini, C.F., 2005. Vertical stratification and air-sea CO_2 fluxes in the Patagonian shelf. J. Geophys. Res. COcean. 110, 1–10. https://doi.org/10.1029/2004JC002488.

Bianchi, A.A., Pino, D.R., Osiroff, A.P., Segura, V., Lutz, V., Clara, M.L., Balestrini, C.F., Piola, A.R., 2009. Annual balance and seasonal variability of sea-air CO_2 fluxes in the Patagonia Sea: their relationship with fronts and chlorophyll distribution. J. Geophys. Res. 114, 1–11. https://doi.org/10.1029/2008JC004854.

Biddle, L.C., Kaiser, J., Heywood, K.J., Thompson, A.F., Jenkins, A., 2015. Ocean glider observations of iceberg-enhanced biological production in the northwestern Weddell Sea. Geophys. Res. Lett. 42 (2), 459–465.

Björck, S., Lambeck, K., Möller, P., Waldmann, N., Bennike, O., Jiang, H., Li, D., Sandgren, P., Nielsen, A.B., Porter, C.T., 2021. Relative sea level changes and glacio-isostatic modelling in the Beagle Channel, Tierra del Fuego, Chile: glacial and tectonic implications. Quat. Sci. Rev. 251 https://doi.org/10.1016/j.quascirev.2020.106657.

Borges, A.V., Delille, B., Frankignoulle, M., 2005. Budgeting sinks and sources of CO_2 in the coastal ocean: diversity of ecosystem counts. Geophys. Res. Lett. 32, 1–4. https://doi.org/10.1029/2005GL023053.

Borges, A.V., Schiettecatte, L.S., Abril, G., Delille, B., Gazeau, F., 2006. Carbon dioxide in European coastal waters. Estuar. Coast. Shelf Sci. 70, 375–387. https://doi.org/10.1016/j.ecss.2006.05.046.

Boyd, P.W., 2002. Environmental factors controlling phytoplankton processes in the Southern Ocean. J. Phycol. 38, 844–861. https://doi.org/10.1046/j.1529-8817.2002.t01-1-01203.x.

Breitburg, D., Levin, L.A., Oschlies, A., Grégoire, M., Chavez, F.P., Conley, D.J., Garçon, V., Gilbert, D., Gutiérrez, D., Isensee, K., Jacinto, G.S., Limburg, K.E., Montes, I., Naqvi, S.W.A., Pitcher, G.C., Rabalais, N.N., Roman, M.R., Rose, K.A., Seibel, B.A., Telszewski, M., Yasuhara, M., Zhang, J., 2018. Declining oxygen in the global ocean and coastal waters. Science (80) 359, eaam7240. https://doi.org/10.1126/science.aam7240.

Bujalesky, G.G., 2011. The flood of the Beagle Valley (11,000 YR B.P.), Tierra del Fuego. An. del Inst. la Patagon. 39, 5–21. https://doi.org/10.4067/s0718-686x2011000100001.

Bujalesky, G., Aliotta, S., Isla, F., 2004. Facies del subfondo del canal Beagle, Tierra del Fuego. Rev. la Asoc. Geol. Argentina 59, 29–37.

Butterworth, B.J., Miller, S.D., 2016. Automated underway eddy covariance system for air-sea momentum, heat, and CO_2 fluxes in the Southern Ocean. J. Atmos. Ocean. Technol. 33, 635–652. https://doi.org/10.1175/JTECH-D-15-0156.1.

Caetano, L.S., Pollery, R.C.G., Kerr, R., Magrani, F., Ayres Neto, A., Vieira, R., Marotta, H., 2020. High-resolution spatial distribution of pCO_2 in the coastal Southern Ocean in late spring. Antarct. Sci. 32, 476–485. https://doi.org/10.1017/S0954102020000334.

Cai, W.J., Hu, X., Huang, W.J., Jiang, L.Q., Wang, Y., Peng, T.H., Zhang, X., 2010. Alkalinity distribution in the western North Atlantic Ocean margins. J. Geophys. Res. Ocean. 115, 1–15. https://doi.org/10.1029/2009JC005482.

Cao, Z., Yang, W., Zhao, Y., Guo, X., Yin, Z., Du, C., Zhao, H., Dai, M., 2020. Diagnosis of CO_2 dynamics and fluxes in global coastal oceans. Natl. Sci. Rev. 7, 786–797. https://doi.org/10.1093/nsr/nwz105.

Carvalho, A.C.O., Kerr, R., Mendes, C.R.B., Azevedo, J.L.L., Tavano, V.M., 2020. Phytoplankton strengthen CO_2 uptake in the South Atlantic Ocean. Prog. Oceanogr. 102476 https://doi.org/10.1016/j.pocean.2020.102476.

Cole, J.J., Caraco, N.F., 1998. Atmospheric exchange of carbon dioxide in a low-wind oligotrophic lake measured by the addition of SF6. Limnol. Oceanogr. 43, 647–656. https://doi.org/10.4319/lo.1998.43.4.0647.

Conley, D.J., Carstensen, J., Ærtebjerg, G., Christensen, P.B., Dalsgaard, T., Hansen, J.L. S., Josefson, A.B., 2007. Long-term changes and impacts of hypoxia in Danish coastal waters. Ecol. Appl. 17, 165–184. https://doi.org/10.1890/05-0766.1.

Coronato, F.R., 1993. Wind chill factor applied to Patagonian climatology. Int. J. Biometeorol. 37, 1–6. https://doi.org/10.1007/BF01212759.

Cucco, A., Martín, J., Quattrocchi, G., Fenco, H., Umgiesser, G., Fernandez, D.A., 2022. Water circulation and transport time scales in the Beagle Channel, southernmost tip of South America. J. Mar. Sci. Eng. 10, 941. https://doi.org/10.3390/jmse10070941.

Dávila, P.M., Figueroa, D., Müller, E., 2002. Freshwater input into the coastal ocean and its relation with the salinity distribution off austral Chile (35-55°s). Cont. Shelf Res. 22, 521–534. https://doi.org/10.1016/S0278-4343(01)00072-3.

De Muro, S., Tecchiato, S., Porta, M., Buosi, C., Ibba, A., 2018. Geomorphology of marine and glacio-lacustrine terraces and raised shorelines in the northern sector of Península Brunswick, Patagonia, straits of Magellan, Chile. J. Maps 14, 135–143. https://doi.org/10.1080/17445647.2018.1441759.

Delille, B., Vancoppenolle, M., Geilfus, N.-X., Tilbrook, B., Lannuzel, D., Schoemann, V., Becquevort, S., Carnat, G., Delille, D., Lancelot, C., Chou, L., Dieckmann, G.S., Tison, J.-L., 2014. Southern Ocean CO_2 sink: the contribution of the sea ice. J. Geophys. Res. Ocean. 119, 6340–6355. https://doi.org/10.1002/2014JC009941. Received.

Dickson, A.G., Sabine, C.L., Christian, J.R., 2007. Guide to best practices for ocean CO_2 measurements. North Pacific Marine Science Organization, 3. PICES Special Publication, p. 191.

Diez, M.J., Cabreira, A.G., Madirolas, A., Martín, J., Scioscia, G., Schiavini, A., et al., 2018. Winter is cool: spatio-temporal patterns of the squat lobster Munida gregaria and the Fuegian sprat Sprattus fuegensis in a sub-Antarctic estuarine environment. Polar Biol. 41, 2591–2605. https://doi.org/10.1007/s00300-018 -2394-2.

D'Onofrio, E.E., Oreiro, F.A., Grismeyer, W.H., Fiore, M.M.E., 2016. Predicciones precisas de marea astronómica calculadas a partir de altimetría satelital y observaciones costeras para la zona de Isla Grande de Tierra del fuego, ISLAs de los Estados y Canal de Beagle. Geoacta (Argentina) 40, 60–75.

Duarte, C.M., Agustí, S., Augustí, S., 1998. The CO_2 balance of unproductive aquatic ecosystems. Science (80) 281, 234–236. https://doi.org/10.1126/science.281.5374.234.

Erickson, Z.K., Thompson, A.F., 2018. The seasonality of physically driven export at submesoscales in the northeast Atlantic Ocean. Glob. Biogeochem. Cycles 32 (8), 1144–1162.

Flores Melo, X., Martín, J., Kerdel, L., Bourrin, F., Colloca, C.B., Menniti, C., de Madron, X.D., 2020. Particle dynamics in Ushuaia Bay (Tierra del Fuego)-potential effect on dissolved oxygen depletion. Water 12, 324. https://doi.org/10.3390/w12020324.

Frankignoulle, M., Borges, A.V., 2001. Direct and indirect pCO_2 measurements in a wide range of pCO_2 and salinity values (the Scheldt estuary). Aquat. Geochemistry 7, 267–273.

Friedlingstein, P., O'Sullivan, M., Jones, M.W., Andrew, R.M., Hauck, J., Olsen, A., Peters, G.P., Peters, W., Pongratz, J., Sitch, S., Le Quéré, C., Canadell, J.G., Ciais, P., Jackson, R.B., Alin, S., Aragão, L.E.O.C., Arneth, A., Arora, V., Bates, N.R., Becker, M., Benoit-Cattin, A., Bittig, H.C., Bopp, L., Bultan, S., Chandra, N., Chevallier, F., Chini, L.P., Evans, W., Florentie, L., Forster, P.M., Gasser, T., Gehlen, M., Gilfillan, D., Gkritzalis, T., Gregor, L., Gruber, N., Harris, I., Hartung, K., Haverd, V., Houghton, R.A., Ilyina, T., Jain, A.K., Joetzjer, E., Kadono, K., Kato, E., Kitidis, V., Korsbakken, J.I., Landschützer, P., Lefèvre, N., Lenton, A., Lienert, S., Liu, Z., Lombardozzi, D., Marland, G., Metzl, N., Munro, D.R., Nabel, J.E.M.S., Nakaoka, S.I., Niwa, Y., O'Brien, K., Ono, T., Palmer, P.I., Pierrot, D., Poulter, B., Resplandy, L., Robertson, E., Rödenbeck, C., Schwinger, J., Séférian, R., Skjelvan, I., Smith, A.J.P., Sutton, A.J., Tanhua, T., Tans, P.P., Tian, H., Tilbrook, B., Van Der Werf, G., Vuichard, N., Walker, A.P., Wanninkhof, R., Watson, A.J., Willis, D., Wiltshire, A.J., Yuan, W., Yue, X., Zaehle, S., 2020. Global carbon budget 2020. Earth Syst. Sci. Data 12, 3269–3340. https://doi.org/10.5194/essd-12-3269-2020.

Gaiero, D.M., Probst, J.L., Depetris, P.J., Bidart, S.M., Leleyter, L., 2003. Iron and other transition metals in Patagonian riverborne and windborne materials: geochemical control and transport to the southern South Atlantic Ocean. Geochim. Cosmochim. Acta 67, 3603–3623. https://doi.org/10.1016/S0016-7037(03)00211-4.

Garcia, C.A.E., Garcia, V.M.T., 2008. Variability of chlorophyll-a from ocean color images in the La Plata continental shelf region. Cont. Shelf Res. 28, 1568–1578. https://doi.org/10.1016/j.csr.2007.08.010.

Garreaud, R., Lopez, P., Minvielle, M., Rojas, M., 2013. Large-scale control on the Patagonian climate. J. Clim. 26, 215–230. https://doi.org/10.1175/JCLI-D-12-00001.1.

Garzón-Cardona, J.E., Martinez, A.M., Barrera, F., Pfaff, F., Koch, B.P., Freije, R.H., Gomez, E.A., Lara, R.J., 2016. The Pacific-Atlantic connection: biogeochemical signals in the southern end of the argentine shelf. J. Mar. Syst. 163, 95–101.

Giesecke, R., Martín, J., Piñones, A., Höfer, J., Garcés-Vargas, J., Flores-Melo, X., Alarcón, E., Durrieu de Madron, X., Bourrin, F., González, H.E., 2021. General hydrography of the Beagle Channel, a subantarctic interoceanic passage at the

southern tip of South America. Front. Mar. Sci. 8, 621822 https://doi.org/10.3389/fmars.2021.621822.
Gonzalez, A.M., Paranhos, R., Lutterbach, M.S., 2010. Relationships between fecal indicators and pathogenic microorganisms in a tropical lagoon in Rio de Janeiro, Brazil. Environ. Monit. Assess. 164, 207–219. https://doi.org/10.1007/s10661-009-0886-9.
Grasshoff, K., Kremling, K., Ehrhardt, M., 2009. Methods of Seawater Analysis. John Wiley & Sons.
Gruber, N., 2014. Ocean biogeochemistry: carbon at the coastal interface. Nature advance on 148–149. https://doi.org/10.1038/nature14082.
Guan, Y., Hohn, S., Wild, C., Merico, A., 2020. Vulnerability of global coral reef habitat suitability to ocean warming, acidification and eutrophication. Glob. Chang. Biol. 26, 5646–5660. https://doi.org/10.1111/gcb.15293.
Hamamé, M., Antezana, T., 1999. Chlorophyll and zooplankton in microbasins along the straits of the Magellan-Beagle Channel passage. Sci. Mar. 63, 35–42. https://doi.org/10.3989/scimar.1999.63s135.
Hoegh-Guldberg, O., Mumby, P.J., Hooten, A.J., Steneck, R.S., Greenfield, P., Gomez, E., Harvell, C.D., Sale, P.F., Edwards, A.J., Caldeira, K., Knowlton, N., Eakin, C.M., Iglesias-Prieto, R., Muthiga, N., Bradbury, R.H., Dubi, A., Hatziolos, M.E., 2007. Coral reefs under rapid climate change and ocean acidification. Science (80) 318, 1737–1742. https://doi.org/10.1126/science.1152509.
Iriarte, J.L., 2018. Natural and human influences on marine processes in Patagonian subantarctic coastal waters. Front. Mar. Sci. 5, 1–7. https://doi.org/10.3389/fmars.2018.00360.
Ito, R.G., Tavano, V.M., Rafael, C., Mendes, B., Eiras, C.A., 2017. Sea-air CO_2 fluxes and pCO_2 variability in the Northern Antarctic Peninsula during 3 summer periods (2008−2010). Deep. Res. Part II. https://doi.org/10.1016/j.dsr2.2017.09.004.
Iturraspe, R.J., Sottini, R., Schroeder, C., Escobar, J., 1989. Hidrología y variables climáticas del Territorio de Tierra del Fuego. Información básica. Contrib. Científica. CADIC 7 (196 pp).
Jacob, B.G., Tapia, F.J., Daneri, G., Iriarte, J.L., Montero, P., Sobarzo, M., Quiñones, R.A., 2014. Springtime size-fractionated primary production across hydrographic and PAR-light gradients in Chilean Patagonia (41-50°S). Prog. Oceanogr. 129, 75–84. https://doi.org/10.1016/j.pocean.2014.08.003.
Jiang, L.Q., Cai, W.J., Wang, Y., 2008. A comparative study of carbon dioxide degassing in river- and marine-dominated estuaries. Limnol. Oceanogr. 53, 2603–2615. https://doi.org/10.4319/lo.2008.53.6.2603.
Joesoef, A., Huang, W.J., Gao, Y., Cai, W.J., 2015. Air-water fluxes and sources of carbon dioxide in the Delaware Estuary: spatial and seasonal variability. Biogeosciences 12, 6085–6101. https://doi.org/10.5194/bg-12-6085-2015.
Kahl, L.C., Bianchi, A.A., Paula, A., Pino, D.R., Piola, A.R., 2017. Distribution of sea-air CO_2 fluxes in the Patagonian Sea: seasonal, biological and thermal effects. Cont. Shelf Res. 1–7 https://doi.org/10.1016/j.csr.2017.05.011.
Kerr, R., Orselli, I.B.M., Lencina-avila, J.M., Eidt, R.T., Mendes, R.B., Leticia, C., Goyet, C., Mata, M.M., Tavano, M., Mendes, C.R., Cotrim, L., Goyet, C., Tavano, V. M., 2017. Carbonate system properties in the Gerlache Strait, Northern Antarctic Peninsula (February 2015): I. Sea – Air CO_2 fluxes. Deep. Res. Part II, 1–11. https://doi.org/10.1016/j.dsr2.2017.02.008.
Laruelle, G.G., Cai, W.-J., Hu, X., Gruber, N., Mackenzie, F.T., Regnier, P., 2018. Continental shelves as a variable but increasing global sink for atmospheric carbon dioxide. Nat. Commun. 9, 454. https://doi.org/10.1038/s41467-017-02738-z.
Libes, S., 2011. In: Academic, P. (Ed.), Introduction to Marine Biogeochemistry.
Marotta, H., Duarte, C.M., Guimaraes-Souza, B.A., Enrich-Prast, A., 2012. Synergistic control of CO_2 emissions by fish and nutrients in a humic tropical lake. Oecologia 168 (3), 839–847.
Martin, J., Colloca, C., Diodato, S., Malits, A., Kreps, G., 2016. Variabilidad espacio-temporal de las concentraciones de oxígeno disuelto en Bahía Ushuaia y Canal Beagle (Tierra del Fuego). Nat. Patagónica 8, 193.
Martin, J., Malits, A., de Madron, X.D., Bourrin, F., Melo, X.F., Lovrich, G., 2019. Hydrography, circulation and suspended particle distribution in Ushuaia Bay and the Beagle Channel. Geophys. Res. Abstr. 21 (EGU2019-17635-1).
Monteiro, T., Kerr, R., Machado, E.D.C., 2020a. Seasonal variability of net sea-air CO_2 fluxes in a coastal region of the northern Antarctic Peninsula. Sci. Rep. 10 (1), 1–15.
Monteiro, T., Kerr, R., Orselli, I.B.M., Lencina-Avila, J.M., 2020b. Towards an intensified summer CO_2 sink behaviour in the Southern Ocean coastal regions. Prog. Oceanogr. 183, 102267 https://doi.org/10.1016/j.pocean.2020.102267.
Olson, D.M., Dinerstein, E., Wikramanayake, E.D., Burgess, N.D., Powell, G.V.N., Underwood, E.C., D'Amico, J.A., Itoua, I., Strand, H.E., Morrison, J.C., Loucks, C.J., Allnutt, T.F., Ricketts, T.H., Kura, Y., Lamoreux, J.F., Wettengel, W.W., Hedao, P., Kassem, K.R., 2001. Terrestrial ecoregions of the world: A new map of life on earth. Bioscience 51, 933. https://doi.org/10.1641/0006-3568(2001)051[0933:TEOTWA]2.0.CO2.
Orselli, I.B.M., Kerr, R., Ito, R.G., Tavano, V.M., Mendes, C.R.B., Garcia, C.A.E., 2018. How fast is the Patagonian shelf-break acidifying? J. Mar. Syst. 178, 1–14. https://doi.org/10.1016/j.jmarsys.2017.10.007.
Orúe-Echevarría, D., Pelegrí, J. L., Castellanos, P., Guallar, C., Marotta, H., Marrasé, C., et al., 2020. Dataset on the RETRO-BMC cruise onboard the R/V Hespérides, April 2017, Brazil-Malvinas Confluence. Data in Brief, 30, 105412.
Parente, A., Sutherland, J.C., 2013. Principal component analysis of turbulent combustion data: data pre-processing and manifold sensitivity. Combust. Flame 160, 340–350. https://doi.org/10.1016/j.combustflame.2012.09.016.
Paruelo, J.M., Lauenroth, W.K., Epstein, H.E., Burke, I.C., Aguiar, M.R., Sala, O.E., 1995. Regional climatic similarities in the temperate zones of north and South America. J. Biogeogr. 22, 915. https://doi.org/10.2307/2845992.
Presta, M.L., Xaus, L., Martín, J., Diez, M.J., Lovrich, G.A., Capitanio, F.L., 2022. Spatial distribution of Munida gregaria (Decapoda, Munididae) larvae in the silled Beagle Channel: insights from spring and autumn surveys. J. Mar. Syst. 237, 103815 https://doi.org/10.1016/j.jmarsys.2022.103815.
Prohaska, F., 1976. The climate of argentina, Paraguay and Uruguay. In: Climates of Central and South America, pp. 13–112.
Rabassa, J., 2008. Late Cenozoic Glaciations in Patagonia and Tierra del Fuego. Dev. Quat. Sci. 11, 151–204. https://doi.org/10.1016/S1571-0866(07)10008-7.
Ramos, V.A., 2008. Patagonia: A paleozoic continent adrift? J. S. Am. Earth Sci. 26, 235–251. https://doi.org/10.1016/j.jsames.2008.06.002.
Rignot, E., Rivera, A., Casassa, G., 2003. Contribution of the Patagonia Icefields of South America to Sea Level Rise. Science (80) 302, 434–437. https://doi.org/10.1126/science.1087393.
Saraceno, M., Martín, J., Moreira, D., Pisoni, J.P., Tonini, M.H., 2021. Physical changes in the Patagonian shelf. In: Walter Helbling, E., Narvarte, M.A., González, R.A., Villafañe, V.E. (Eds.), Global Change in Atlantic Coastal Patagonian Ecosystems. Natural and Social Sciences of Patagonia. Springer, Cham. https://doi.org/10.1007/978-3-030-86676-1.
Schlitzer, R., Mieruch, S., 2021. Ocean Data View. https://odv.awi.de.
Schloss, I., Ferreyra, G., Ferrario, M.E., Almandoz, G.O., Codina, R., Alejandro, A., Bianchi, A., 2007. Role of plankton communities in sea – air variations in pCO_2 in the SW Atlantic Ocean. Mar. Ecol. Prog. Ser. 332, 93–106.
Schwarz, J.N., Schodlok, M.P., 2009. Impact of drifting icebergs on surface phytoplankton biomass in the Southern Ocean: ocean colour remote sensing and in situ iceberg tracking. Deep-Sea Res. I Oceanogr. Res. Pap. 56 (10), 1727–1741.
Sievers, A., Silva, N., 2008. Water masses and circulation in austral Chilean channels and fjords. Prog. Oceanogr. 53–58.
Silva, N., Calvete, C., Sievers, H., 1998. Masas de agua y circulación general para algunos canales australes entre Puerto Montt y Laguna San Rafael, Chile (Crucero CIMAR-Fiordo 1). Cienc. Tecnol.Mar. 22, 17–47. https://doi.org/10.4067/s0718-686x2011000200002.
Silva, N., Vargas, C.A., Prego, R., 2011. Land-ocean distribution of allochthonous organic matter in surface sediments of the Chiloé and Aysén interior seas (Chilean Northern Patagonia). Cont. Shelf Res. 31, 330–339. https://doi.org/10.1016/j.csr.2010.09.009.
Smetacek, V., Klaas, C., Strass, V.H., Assmy, P., Montresor, M., Cisewski, B., et al., 2012. Deep carbon export from a Southern Ocean iron-fertilized diatom bloom. Nature 487 (7407), 313–319.
Smith, R.B., Evans, J.P., 2007. Orographic precipitation and water vapor fractionation over the Southern Andes. J. Hydrometeorol. 8, 3–19.
Smith, R.W., Bianchi, T.S., Allison, M., Savage, C., Galy, V., 2015. High rates of organic carbon burial in fjord sediments globally. Nat. Geosci. 8, 450–453. https://doi.org/10.1038/ngeo2421.
Stock, C.A., Dunne, J.P., Fan, S., Ginoux, P., John, J., Krasting, J.P., Laufkötter, C., Paulot, F., Zadeh, N., 2020. Ocean biogeochemistry in GFDL's earth system model 4.1 and its response to increasing atmospheric CO_2. J. Adv. Model. Earth Syst. 12 https://doi.org/10.1029/2019MS002043.
Takahashi, T., Olafsson, J., Goddard, J.G., Chipman, D.W., Sutherland, S.C., 1993. Seasonal variation of CO_2 and nutrients in the high??? Latitude surface oceans: A comparative study. Glob. Biogeochem. Cycles 7, 843–878. https://doi.org/10.1029/93GB02263.
Takahashi, T., Sutherland, S.C., Sweeney, C., Poisson, A., Metzl, N., Tilbrook, B., Bates, N., Wanninkhof, R., Feely, R.A., Sabine, C., Olafsson, J., Nojiri, Y., 2002. Global sea – air CO_2 flux based on climatological surface ocean pCO_2, and seasonal biological and temperature effects. Deep Sea Res Part II Top. Stud. Oceanogr. 49, 1601–1622. https://doi.org/10.1016/S0967-0645(02)00003-6.
Thomas, H., Bozec, Y., Elkalay, K., De Baar, H.J.W., 2004. Enhanced open ocean storage of CO_2 from shelf sea pumping. Science (80) 304, 1005–1008. https://doi.org/10.1126/science.1095491.
Torres, R., Pantoja, S., Harada, N., González, H.E., Daneri, G., Frangopulos, M., Fukasawa, M., 2011. Air-sea CO_2 fluxes along the coast of Chile: From CO_2 outgassing in central northern upwelling waters to CO_2 uptake in southern Patagonian fjords. J. Geophys. Res. Oceans 116, C9.
Torres, R., Alarcón, E., Reid, B., 2021. Simultaneous CO_2 and O_2 supersaturation in waters of Southern Patagonia? The importance of evaluating overall carbonate system parameters uncertainty and external consistency. A comment to Vargas et al., 2018. Journal of Geophysical Research Biogeosciences 126 (7) (e2019JG005523).
Vergara-Jara, M.J., DeGrandpre, M.D., Torres, R., Beatty, C.M., Cuevas, L.A., Alarcón, E., Iriarte, J.L., 2019. Seasonal changes in carbonate saturation state and Air-Sea CO_2 fluxes during an annual cycle in a stratified-Temperate Fjord (Reloncaví Fjord, Chilean Patagonia). J. Geophys. Res. Biogeosci. 124, 2851–2865. https://doi.org/10.1029/2019JG005028.
Wanninkhof, R., 2014. Relationship between wind speed and gas exchange over the ocean revisited. Limnol. Oceanogr. Methods 12, 351–362. https://doi.org/10.4319/lom.2014.12.351.
Weiss, R.F., 1974. Carbon dioxide in water and seawater: the solubility of a non-ideal gas. Mar. Chem. 2, 203–215. https://doi.org/10.1016/0304-4203(74)90015-2.
Yentsch, C.S., Menzel, D.W., 1963. A method for the determination of phytoplankton chlorophyll and phaeophytin by fluorescence. Deep-Sea Res. Oceanogr. Abstr. 10 (3), 221–231. https://doi.org/10.1016/0011-7471(63)90358-9.
Zar, J.H., 2010. Biostatistical Analysis, 3rd. ed. Prentice Hall, New Jersey.